JUN 24 1965

C

B

Coordinated Science Laboratory

UNIVERSITY OF ILLINOIS – URBANA, ILLINOIS

UNIVERSITY OF ILLINOIS
COORDINATED SCIENCE LABORATORY
URBANA, ILLINOIS

September 30, 1964

PLASMA PHYSICS

FINAL TECHNICAL SUMMARY REPORT

For the Period Ending Sept. 30, 1964

in accordance with Article 1 Item 4c of

Contract DA 28 043 AMC 00073 (E)

PLASMA PHYSICS

FINAL TECHNICAL SUMMARY REPORT

For the Period Ending Sept. 30, 1964 in
accordance with Article 1 Item 4c of
Contract DA 28 043 AMC 00073 (E)

<u>ERRATA</u>

Figure 7 on page 13 should be Figure 10 on page 17 and Figure 10
on page 17 should be Figure 7 on page 13.

The titles are correct.

I. INTRODUCTION

The objective of these experiments was to study the inter-
action of a strong electron beam with a high density plasma with
emphasis on two aspects: 1) the demonstration of the hose instability,
and 2) the possibility of quenching the electrostatic instability by a
sufficiently large velocity spread. Since the growth rate for the
electrostatic instability greatly exceeds that for the hose instability,
que. ".ing of the electrostatic instability was a necessary prerequisite
for any study of the hose instability.

A parameter study[1] was conducted which showed that it should
be possible to observe the hose instability with a rather modest elec-
tron beam. The conditions underlying the theory of the hose instability
are summarized in Table I. A 3 amp, 25 kV electron beam is assumed.

TABLE I.

	$r = 1$ mm	$r = 2$ mm
$\omega + kv < \omega_b$ Rigid motion of the beam	$\omega < 3 \times 10^9$	$\omega < 1.5 \times 10^9$
$\dfrac{4\pi\sigma\omega r^2}{c^2} \ll 1$ Plasma not frozen to field lines	$\sqrt{\dfrac{\omega}{\nu_c}} \cdot \omega_p \ll 3 \times 10^{11}$	$\sqrt{\dfrac{\omega}{\nu_c}} \cdot \omega_p \ll 1.5 \times 10^{11}$
$\sigma \gg vk, \omega$ Conduction current large com- pared to displacement current	$\omega_p \gg \omega$	$\omega_p \gg \omega$
$\dfrac{4\pi\sigma r}{c} \cdot \dfrac{v}{c} \gg 1$ Magnetic hose instability dominates electrostatic hose instability	$T \gg 200^{\circ}$K and coulomb collisions dominant	$T \gg 70^{\circ}$K

The possibility of quenching the electrostatic instability has been discussed by Ascoli,[2] who derived the following stability criterion:

$$\nu_c > \pi \frac{\omega_b^2}{\omega_p} \left(v_z^2 \frac{\partial f}{\partial v_z} \right)_{max}$$

where ω_B is the plasma frequency of the beam, and ω_p the plasma frequency in the plasma. Assuming a displaced maxwellian distribution function for the beam,

$$f(v_z) = \frac{1}{\sqrt{2\pi} \, \Delta v_z} e^{-\frac{(v_z - v_{zo})^2}{2\Delta v_z^2}}$$

the criterion becomes

$$\nu_c > \sqrt{\frac{\pi}{2e}} \frac{\omega_B^2}{\omega_p} \left(\frac{v_z}{\Delta v_z} \right)^2$$

For an electron beam accelerated by a constant potential, V, the distribution function is given by

$$f(v_z) = \frac{\beta}{\pi^{1/2}} e^{-\beta^2 \left| v_z^2 - \frac{2eV}{m} \right|}$$

with $\beta^2 = \frac{m}{2kT}$. The velocity spread is given by

$$\Delta v = \frac{\Delta v_o}{2} \cdot \frac{\Delta v_o}{v_o} \qquad \Delta v_o = \frac{1}{\beta}$$

where $v_o^2 = \frac{2eV}{m}$, and it is very much smaller than that for a displaced maxwellian.

We can define an effective longitudinal temperature corresponding to this velocity spread and find

$$kT_{eff} = \frac{1}{8} \frac{(kT)^2}{E}$$

where T is the original temperature before acceleration and E the beam energy. The transverse temperature will not be affected by the acceleration. Consequently, in the reference system of the moving beam, the temperature is very anisotropic. Due to interactions between the beam electrons, this anisotropic temperature distribution will tend to maxwellize. One can estimate the time required for the distribution function to come to equilibrium. Under the condition that electron-electron interactions are the dominant mechanism the relaxation time for this process is given by

$$t_R = (\frac{m}{2\pi})^{1/2} \frac{(kT)^{3/2}}{e^4 n_e \ln\Lambda}$$

where m is the electron mass, e the electron charge, n_e the electron density in the beam, and $\Lambda = \frac{3}{2e^3} \frac{(kT)^{3/2}}{\sqrt{\pi n_e}}$. For a current of 3 amperes at 25 kV, an initial temperature of 5 eV, and a 1 mm beam radius, t_R is approximately 6 microseconds. This time is long compared to the interaction time of the beam with the plasma. Consequently, no equilibrium will be established, and the velocity distribution of the beam will not be a displaced maxwellian. Under these conditions, the stability criterion acquires the modified form

$$\nu_c > \frac{\pi^{1/2}}{4} \frac{\omega_B^2}{\omega_p} (\frac{v_o}{\Delta v})^{3/2}$$

In terms of the original velocity spread, Δv_o, this becomes

$$\nu_c > \sqrt{\frac{\pi}{2}} \frac{\omega_B^2}{\omega_p} (\frac{v_o}{\Delta v_o})^3$$

which is more stringent than Ascoli's original criterion. Any estimate, however, based on these formulas, may not be too realistic for the

following reason: As demonstrated in reference 3,4,5, an electron

beam suffers anomalous energy losses before actually becoming unstable.

This results in an enormous enhancement of the original velocity

spread. This behavior can be understood theoretically through the

work of Drummond and Pines[6] on the quasilinear theory of plasma

oscillations.

II. EXPERIMENTAL SETUP

A. Discharge Tube. The discharge tube consists out of standard

pieces of 4-inch Pyrex tubing (Corning Double-Tough Pyrex pipe) sealed

together by neoprene gaskets. Some of the standard pieces were modi-

fied to allow the insertion of diagnostic devices into the discharge.

Figure 1 shows an over-all view of the discharge tube. Hydrogen was

admitted into the tube from a hydrogen tank via a variable leak through

one of the end flanges. This somewhat unusual gas inlet was necessary

in order to prevent the discharge from striking through the gas supply

line to ground. The discharge tube is evacuated by an 800 liter/sec

4-inch diffusion pump via a 2-meter, 4-inch diameter Pyrex tube. This

large path to the diffusion pump was necessary in order to prevent a

discharge to the grounded pump. The pressure in the discharge tube is

measured by a Bayard-Alpert gauge and a Pirani gauge for the low and

the high pressure regions, respectively.

B. Pulser and Pre-Ionization. Breakdown in the discharge tube is

accomplished by a 10 microsecond, high voltage pulse coupled to the

discharge via a pulse transformer. The pulse generator is of the line

type and capable of delivering pulses up to 20 MW peak power. The
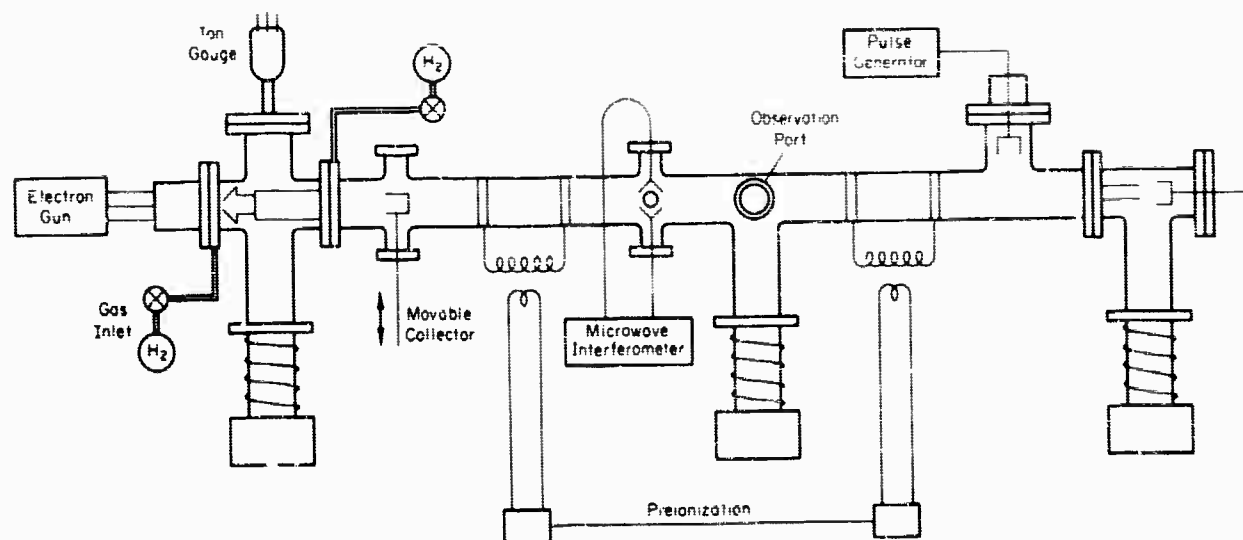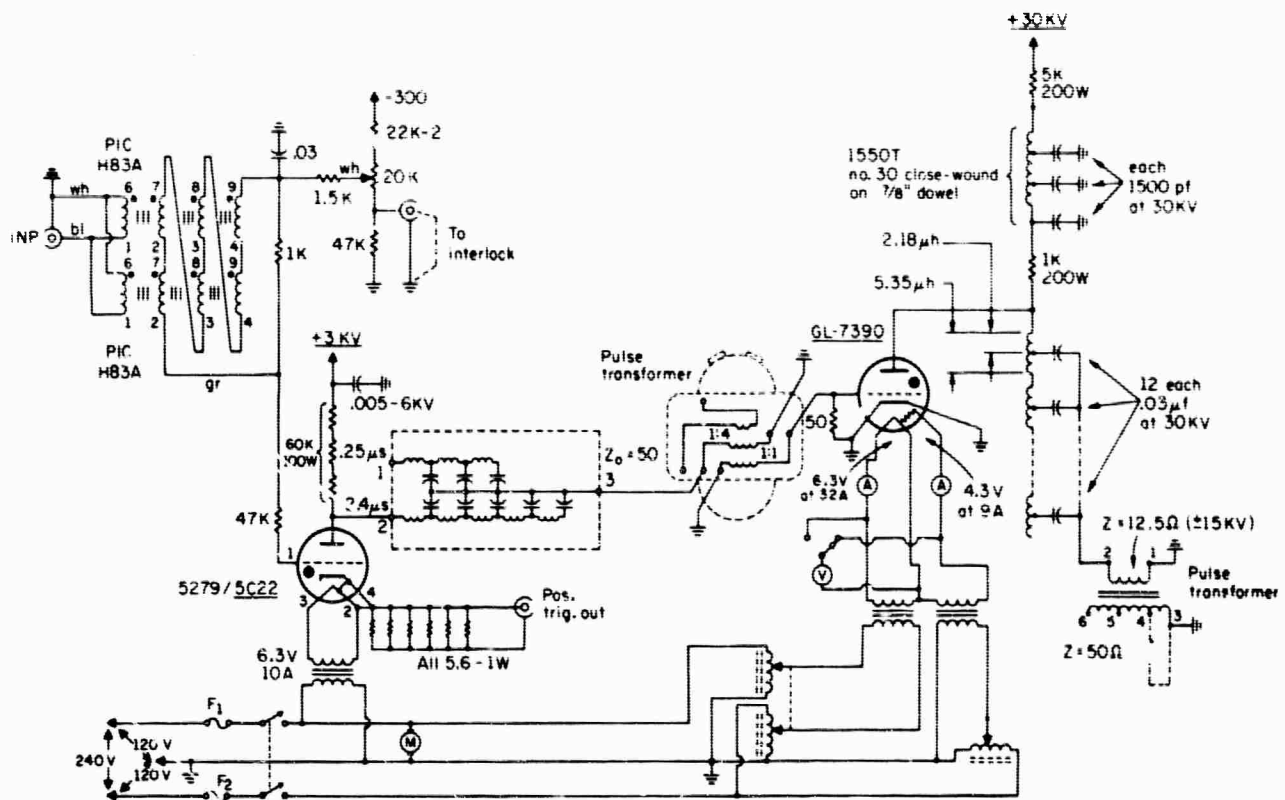
Figure 1.   Over-all View of the Experimental Arrangement.

repetition rate is limited by the high voltage power supply to a maximum
of approximately 20 per second. Figure 2 shows a diagram of the pulse
generator. In order to obtain reproducible discharge conditions, it
was necessary to pre-ionize the gas slightly. This is accomplished by
an 800 μsec, 2 Mc/sec RF pulse coupled capacitatively to four sections
of the discharge tube. A circuit diagram of the RF pre-ionization is
shown in Figure 3.

C. Electron Gun. A hot cathode, magnetically focused arc discharge
was used as an electron source. This type of discharge is known as
v. Ardenne ion source or duo-plasmatron ion source and frequently used
as a source for high ion currents. Fröhlich[7] has modified the basic
ion source design and shown that electron current densities of 500
amperes per square centimeter can be obtained. With a typical extrac-
tion aperture of one square millimeter area, this corresponds to currents
of the order of 5 amperes. Figure 4 shows the construction of the gun.
The essential modification introduced by Fröhlich is an isolated inter-
mediate electrode which gives rise to a space charge field in the
aperture of this electrode. As a result, the electrons are emitted
with large initial energies of the order of 50 eV, which accounts for
the high current densities that can be obtained. Various cathode ma-
terials were used in the gun. The best results were obtained with rhenium
filaments and indirectly heated lanthanum boride cathodes. In order to
obtain a pulsed electron beam, the arc voltage was pulsed while maintain-
ing a constant potential between the extraction electrode and the anode
of the gun. The pulse is obtained from a modified radar pulser. It is
2 μsec long and has an amplitude of the order of 3 kV. Figure 5 shows

Figure 2. Circuit Diagram of High Voltage Pulse Generator.

Figure 3.   Circuit Diagram of RF-Preionization.

Anode

Intermediate
electrode

Filament

Glass
spacer

Magnet
coils

Glass
spacer

Cooling
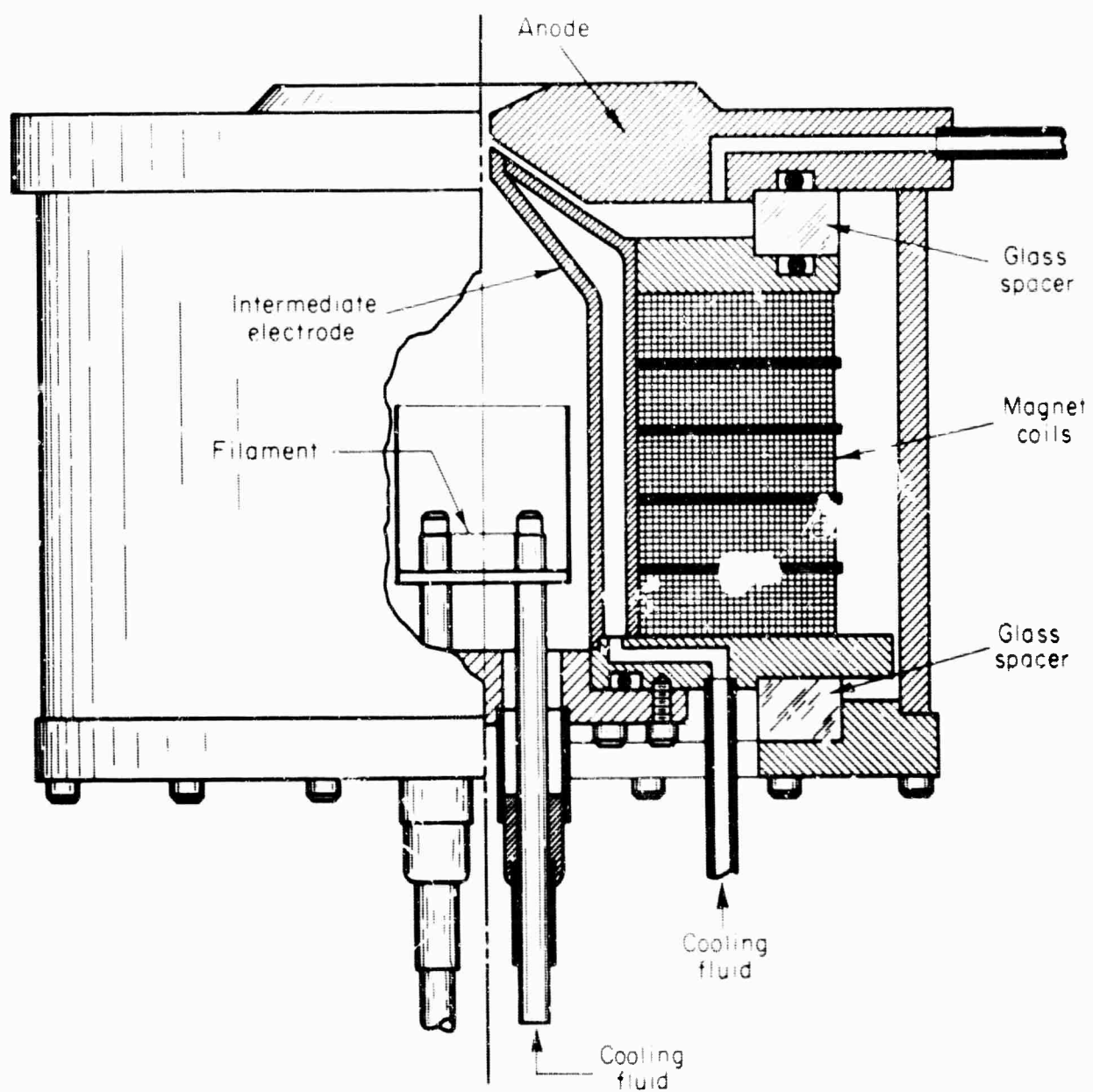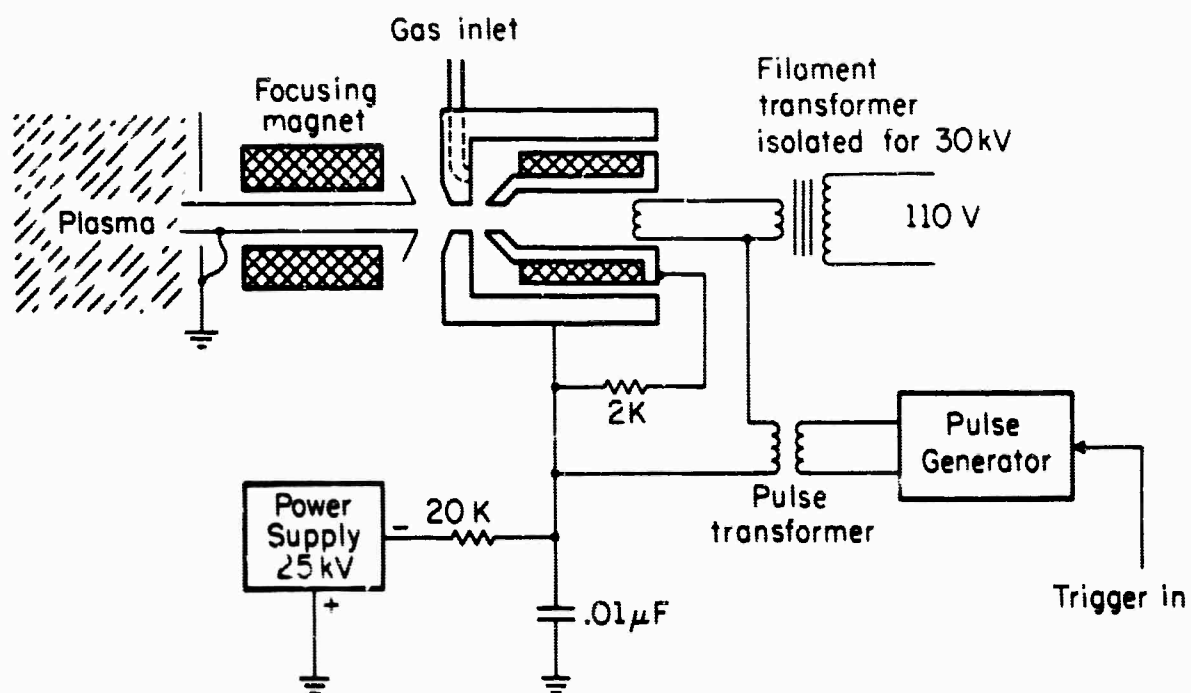fluid

Cooling
fluid

Figure 4.   Electron Source.

Figure 5. Circuit Diagram of Electron Source Power Supply.

a circuit diagram of the electron gun power supply. Figure 6 shows an over-all photograph of the experiment with the discharge in operation.

III. MEASUREMENT OF PLASMA PARAMETERS

A. Electron Density. For the measurement of the electron density, an 8 mm microwave interferometer was constructed. Figure 7 shows a circuit diagram of the setup. The microwave horns are located inside the discharge tube but electrically isolated from the discharge by 1 mil Mylar foils. Two klystrons were used for two different frequency ranges, 36 to 39 kMc/sec, and 26 to 29 kMc/sec. With no discharge on and the klystrons operating CW, the system is tuned to zero signal at the detector. The presence of plasma in the discharge tube upsets the balance and results in a signal at the detector. Figure 8 shows a typical photograph of an oscilloscope trace obtained in this way. The change in amplitude of the interference fringes is due to the attenuation of the microwaves in the plasma. The useful range of electron densities that can be measured this way extends from $10^{12} - 10^{13}/cm^3$, the upper limit being given by the cutoff of the microwaves and the lower limit by the accuracy to which the phase can be determined. Figure 9 shows a set of electron densities as a function of time for different power inputs into the discharge.

B. Electron Collision Frequency. The electron collision frequency can be determined from the attenuation of a microwave signal after passing through the plasma. Since an absolute value of the attenuation has to be determined, precautions have to be taken to assure that only that part of the attenuation is being measured that is due to absorption of microwaves in the plasma. Reflections from the discharge can be
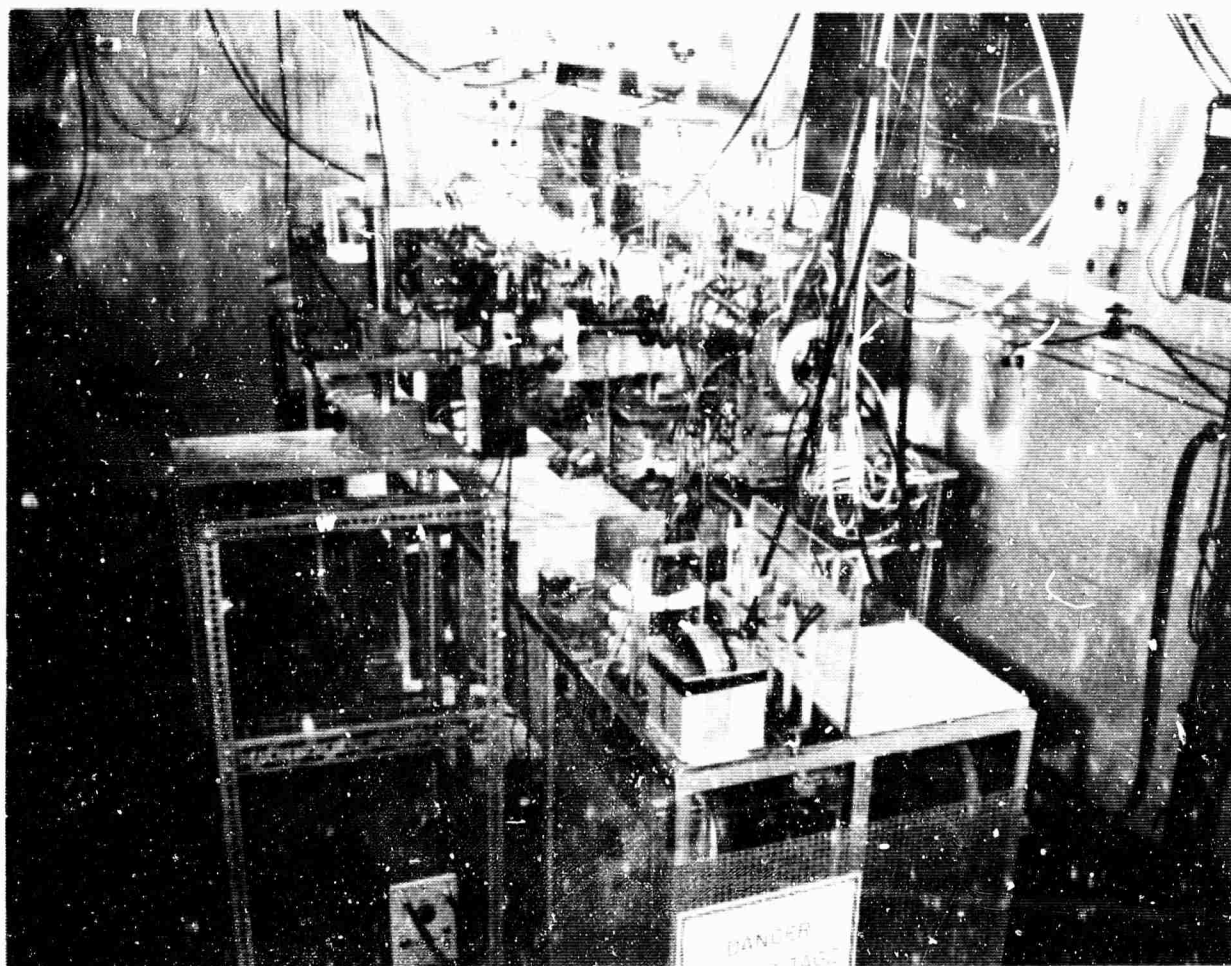
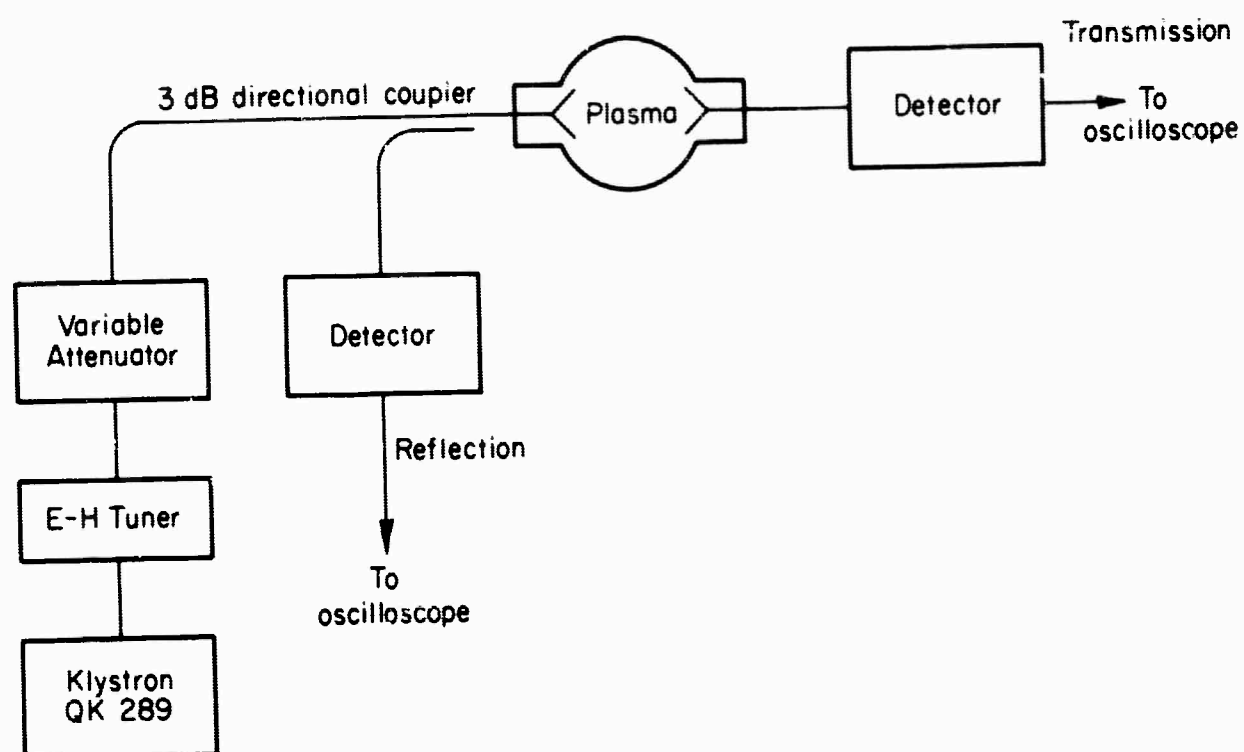Figure 6. Photograph of the Experimental Apparatus.

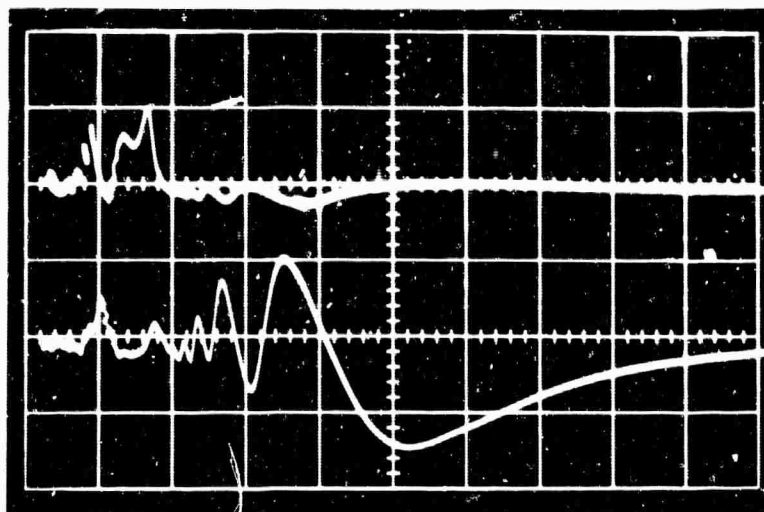Figure 7.   Block Diagram of Microwave Interferometer.

Figure 8. Output of Microwave Interferometer. The upper trace is a
measurement of the reflected power. The signal during the
first 20 μsec is due to transients from the active dis-
charge and has no physical significance.

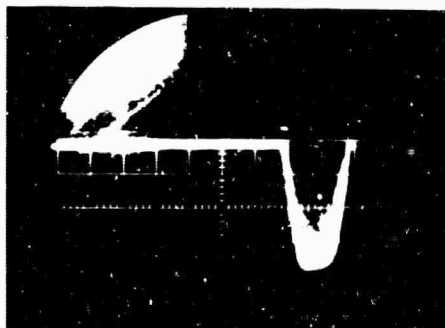Figure 13. Oscilloscope Trace of Electron Beam Current. Maximum
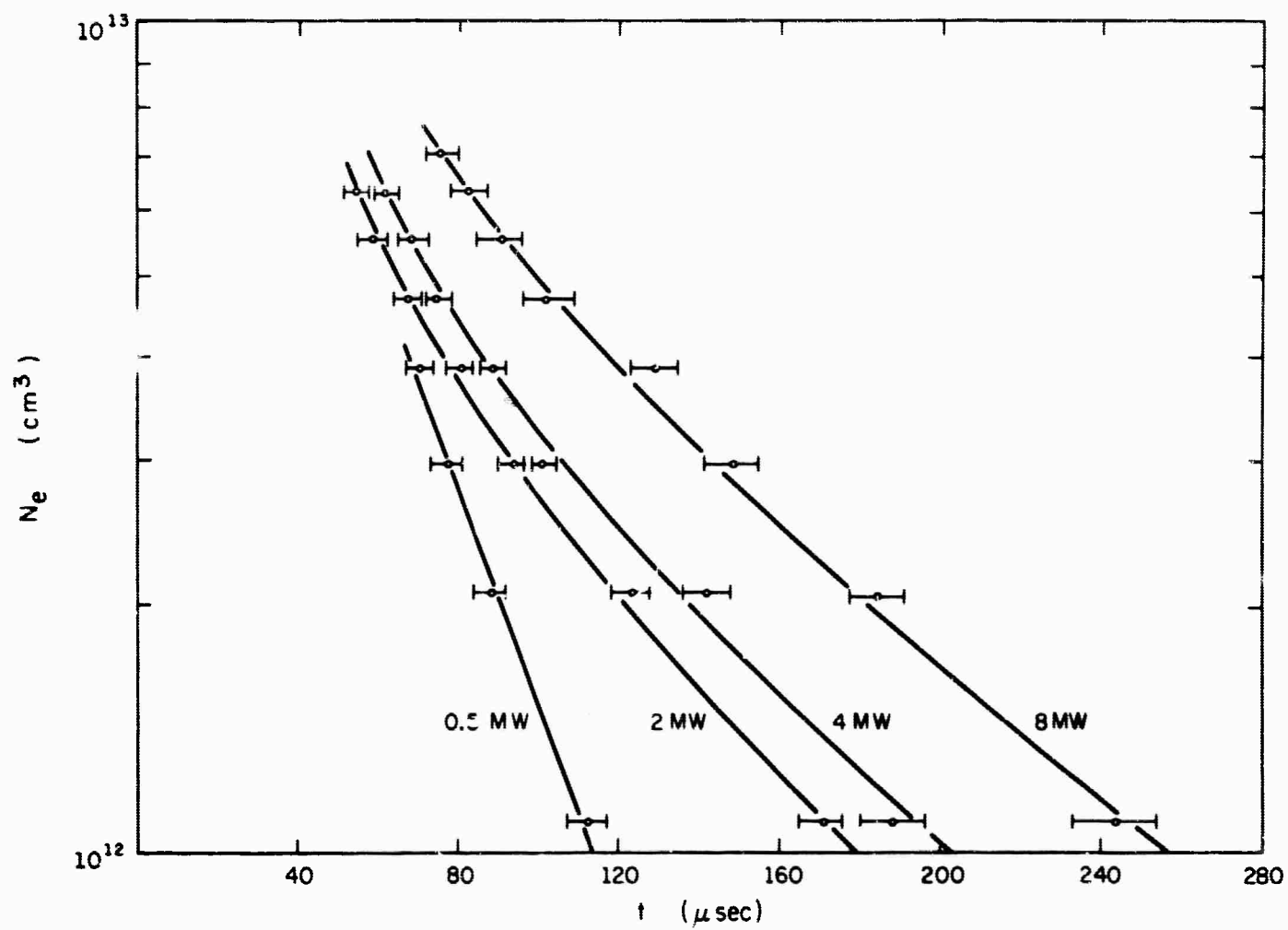current is 0.8 A.

Figure 9.   Electron Density as a Function of Time for Various Power
Inputs.

considerable and greatly distort the measurement. Figure 10 shows a diagram of the circuits used for attenuation measurements. The directional coupler responds to power reflected from the discharge and allows us to estimate the importance of reflections. In the measurements taken with 8 mm microwaves, the reflections were of minor importance. At 1.2 cm wavelength, however, no reliable measurements of the collision frequency were possible. Figure 11 shows values of the collision frequency as a function of time in the discharge. The data show that only Coulomb collisions are important during the times of interest. Calculations of the temperature in the discharge, as determined from the collision frequency. show that the temperature approaches room temperature asymptotically in agreement with what one would expect.

C. Spectrum of the Discharge. A measurement of the discharge spectrum revealed that the Balmer lines are the dominant emission lines. The only noticeable impurity is sodium, originating from the glass walls of the discharge tube.

D. Kerr Cell Measu_ents. Kerr cell measurements permitted us to study the buildup and decay of the discharge as a function of time and to obtain time resolved values for the electron density profile in the discharge. The Kerr cell is Model E-51A, 2 μsec shutter time, manufactured by the Electro-Optics Corporation. Figure 12 shows a sequence of pictures taken through the Kerr cell. During the first few microseconds, the discharge pinches down and then continuously expands, filling the whole discharge tube. Exposure time for the photographs was five minutes at a 20 cps repetition frequency. Some color photographs were taken which showed that the sodium impurities prevail only
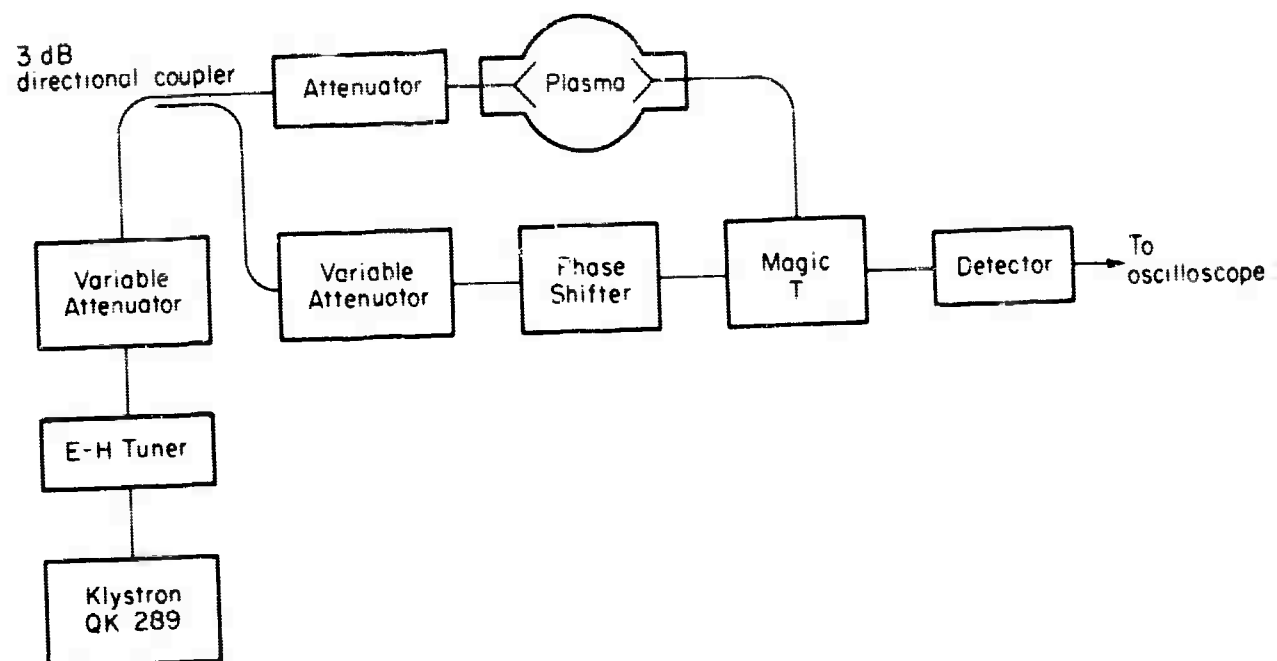
Figure 10. Block Diagram of Microwave Circuit Used for Attenuation Measurements.
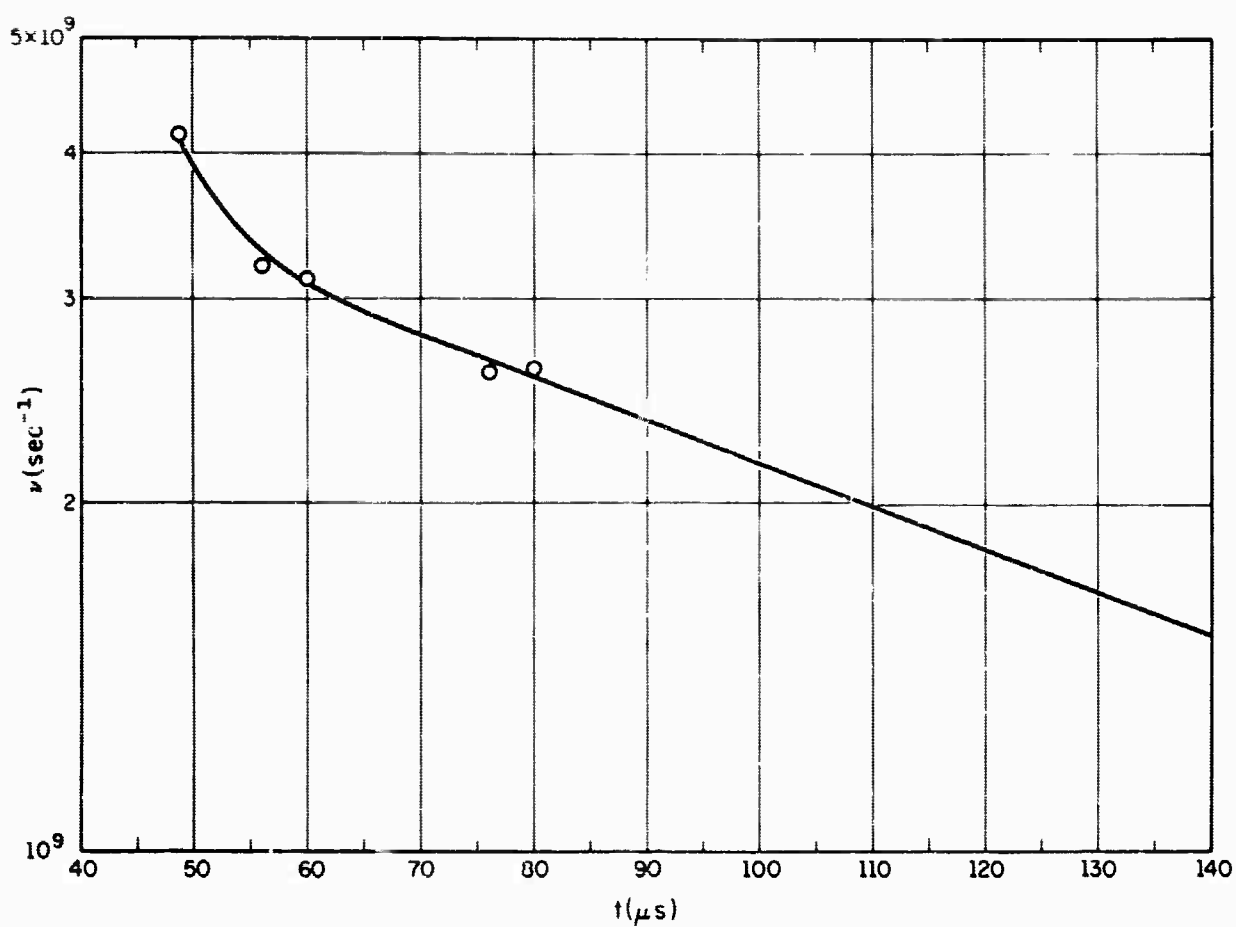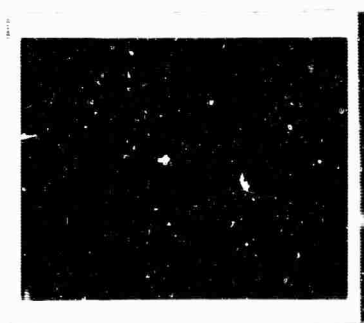
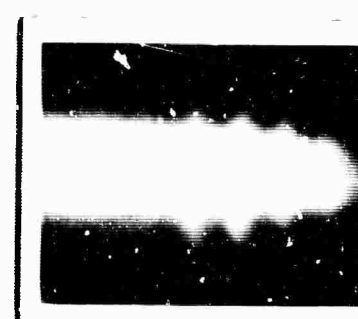Figure 11. Collision Frequency as a Function of Time in the Discharge.

2 μsec   5 μsec

6 μsec   7 μsec   8 μsec
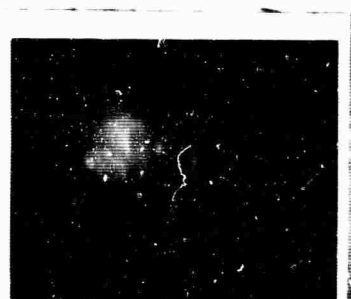
9 μsec   12 μsec   21 μsec
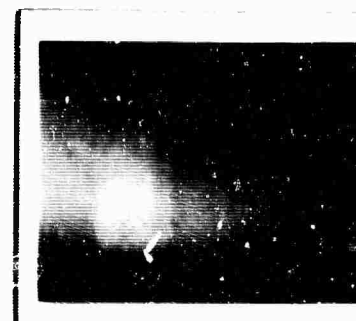
27 μsec   33 μsec

Figure 12. Time-Resolved Photographs of the Discharge. The times refer to the delay with respect to application of the high voltage pulse. See the facing page (p. 19).

during the initial breakdown stage. No sodium lines are apparent in
the recombination light. Time resolved photographs of the discharge
cross section in a region where recombination prevailed permit a cal-
culation of the electron density profile.

IV. BEAM MEASUREMENTS

For measurements of the beam current, a collector was inserted
into the discharge tube a few inches downstream from the entrance
aperture of the beam. During these measurements, the discharge was,
of course, shut off. The collector was connected to an oscilloscope
via a coax cable terminated with 100 Ω. Maximum beam currents of 1 amp
were measured in this way although directly behind the extraction elec-
trode the beam current exceeds 2 amp. The loss of beam current is due
to the fact that the beam has to be guided through a 5 mm diameter,
10 cm long channel in the differential pumping section between the gun
and the discharge tube. Figure 13 shows a typical photograph of an
oscilloscope trace. See Figure 13 on page 14.

Energy Spread of the Beam. In order to get an estimate on
the energy spread of the beam, the diffusion current out of the electron
gun at zero acceleration voltage was analyzed by biasing the collector
with a retarding potential. Figure 14 shows a plot of the collected
current versus the retarding potential. We notice that the average
energy spread of the beam is of the order of 15 eV.

V. MEASUREMENT OF BEAM PLASMA INTERACTION

To study the interaction of the electron beam with the plasma,
the beam was injected into the discharge tube a given time after

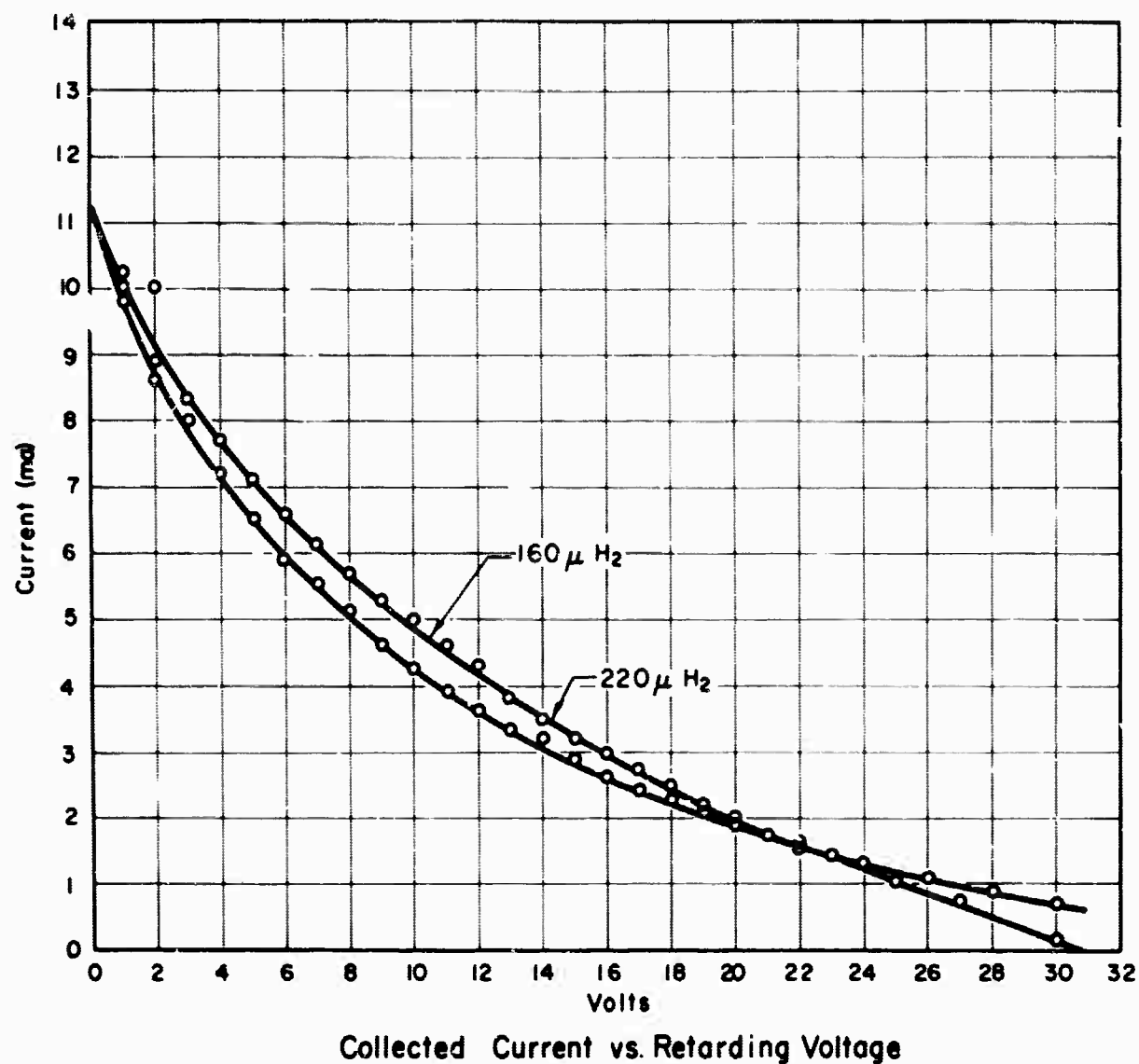Collected Current vs. Retarding Voltage

Figure 14.   Energy Spread of the Beam for Two Different Pressures in
the Electron Gun.

initiation of the discharge. Timing of the different operations was accomplished by several pulse generators and delays connected according to Figure 15. By varying the delay between initiation of the discharge and beam trigger pulse, the electron beam can be exposed to different ambient electron densities. The decay time of the plasma is slow compared to the duration of the pulse so that the beam always sees practically constant electron density. Observing the light output from the discharge, it was realized that the excitation light of the electron beam exceeded the recombination light from the discharge. Hence, the observation of this excitation light was judged to be a convenient diagnostic tool which provided at least a crude indication of the beam behavior. Figure 16 shows an oscilloscope trace of the light output from the discharge with the superimposed excitation light of the beam as measured by a photomultiplier.
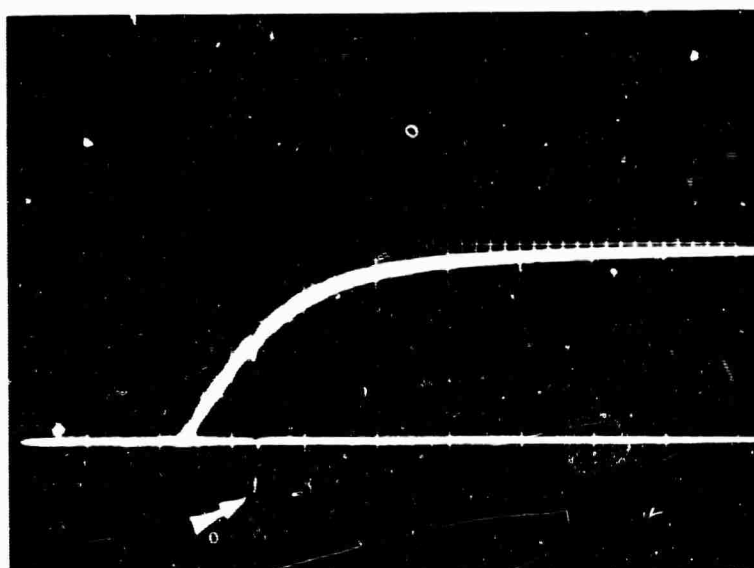
Figure 16. Oscilloscope Trace of Afterglow Light with Superimposed Excitation Light of the Beam. Excitation light of the beam extends down to a value marked by the arrow.
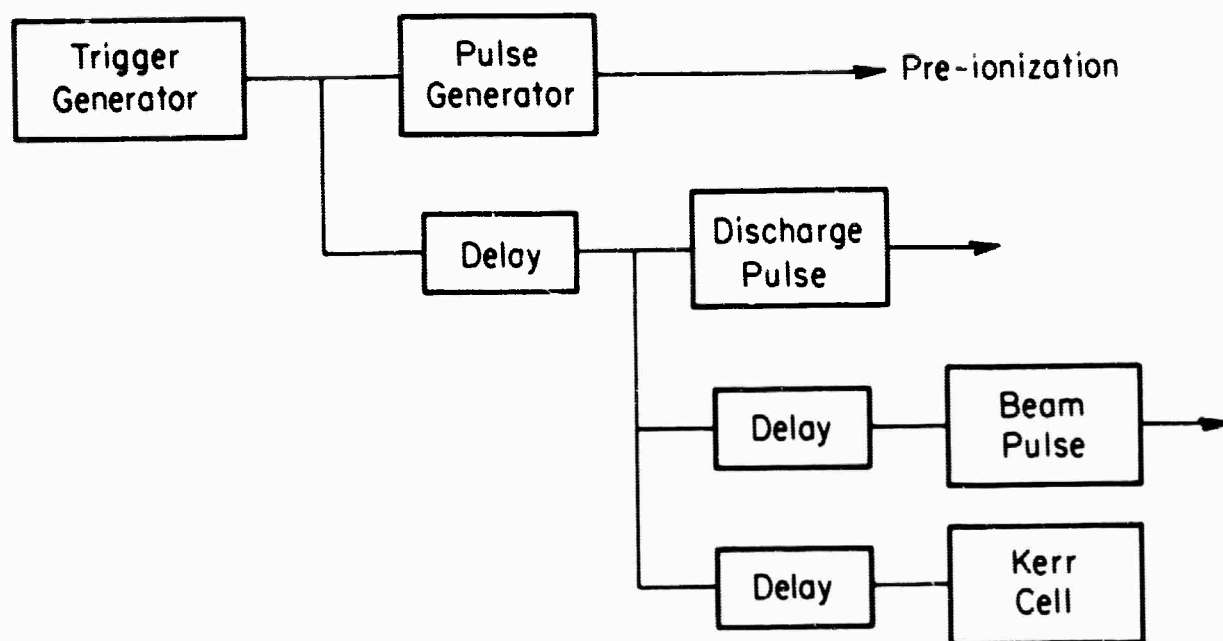
Figure 15. Block Diagram of Timing Circuit.

For a g ven beam current the excitation light suddenly disappeared at a certain plasma density. The disappearance was so sudden that the light intensity decreased to zero within a few microsecond delay time. Systematic measurements were made to establish the relation between electron beam currents and plasma frequency and collision frequency in the plasma at the time of the disappearance of the excitation light. These relations are plotted in Figures 17 and 18. Strangely enough, the observation of the beam current at the collector did not show any sign of instability. The beam penetrated the plasma even at very high plasma densities, and disappeared only at very short delay times corresponding to injection of the beam into active discharge. The nature of this effect is not understood at the present time. Several suggestions can be offered, but none of them seems to be able to explain the phenomenon.

a) At the onset of an instability, anomalous energy losses occur which may heat the plasma. With increasing temperatures, the recombination coefficient decreases and the recombination light decreases also, giving rise to an apparent decrease in excitation light from the beam. What speaks against this explanation is the fact that the excitation light disappeared completely even under conditions where it exceeded the recombination light.

b) Absorption of the excitation light due to an abundant population of excited states can be ruled out. Measurements with an external source of hydrogen lines did not show any absorption.
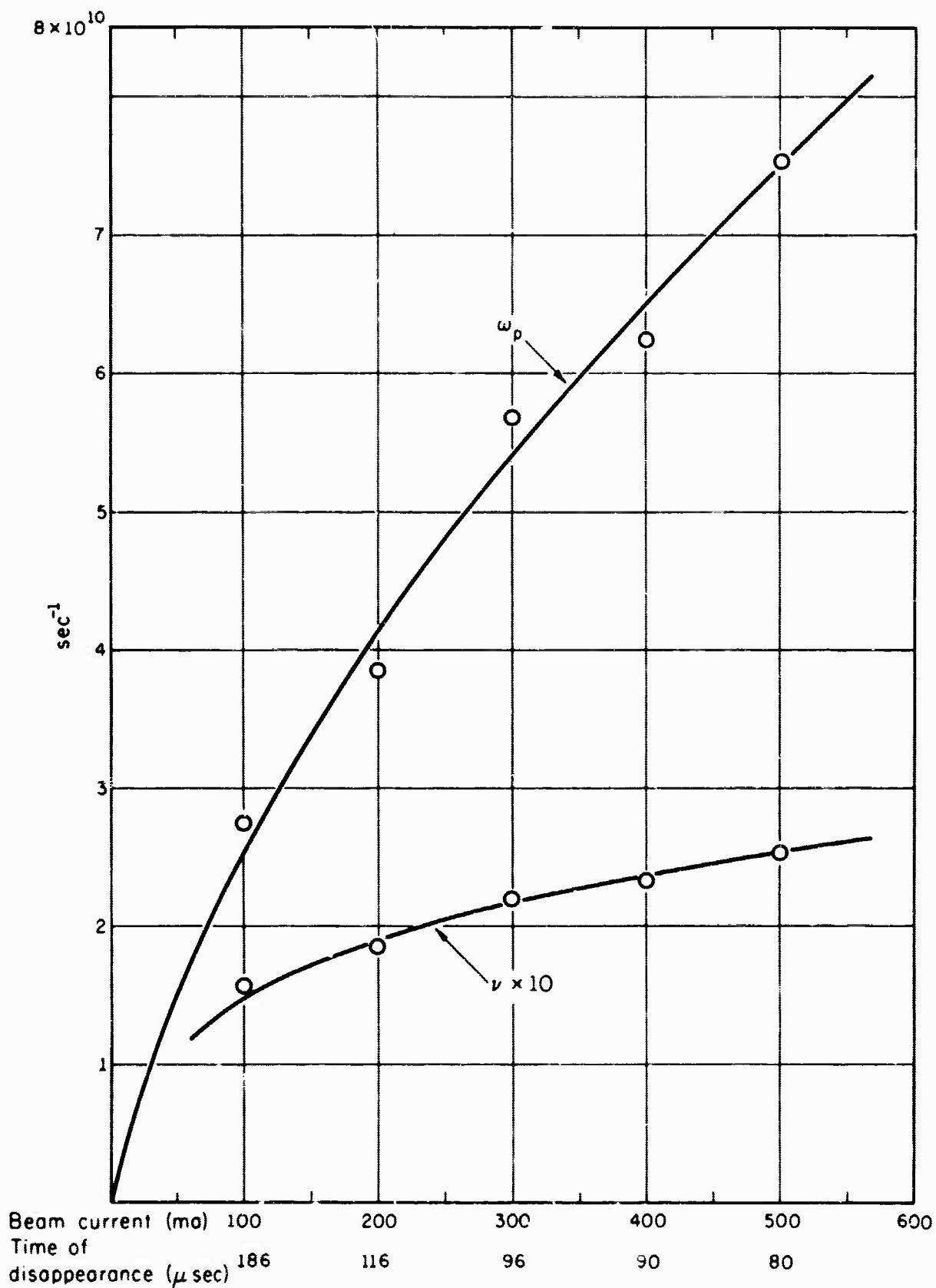
Figure 17. Plasma Frequency and Collision Frequency at the Time of Disappearance of Beam Excitation Light.
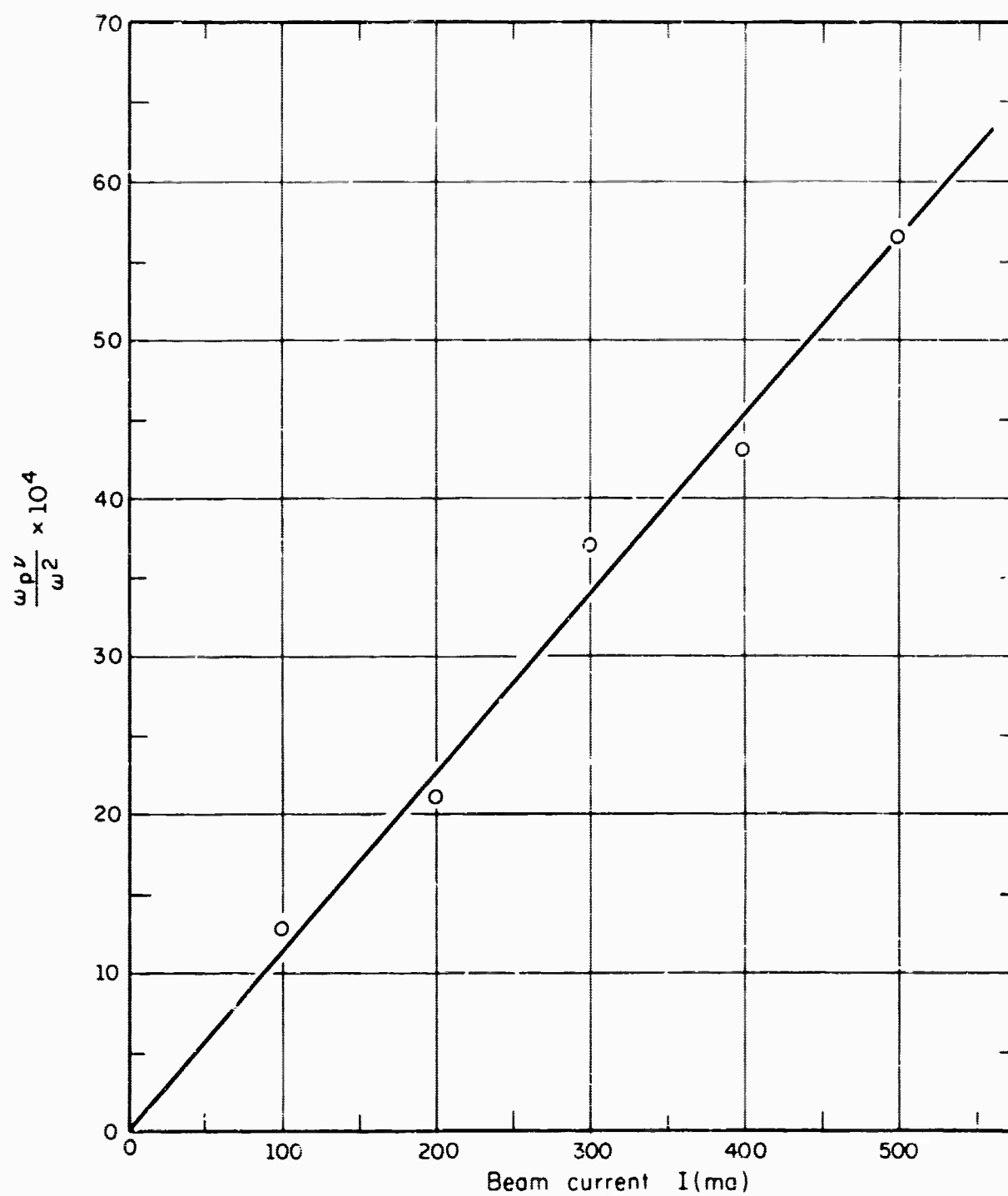
Figure 18. Product of ω_p and ν_c at the Time of Disappearance of Beam Excitation Light Plotted Versus Beam Current.

The beam temperature parameter τ as defined by Singhaus[8] has the value of 0.1 in our experiment. Consequently no collisional quenching of the electrostatic instability should occur. As pointed out in the introduction, however, anomalous energy losses of the beam can occur at the onset of an instability giving rise to such a velocity spread that the condition for collisional quenching is satisfied. This would prevent the instability from growing and result in a stable beam.

If this model is true one can expect a large increase in the magnitude of density fluctuations[9,10] in the plasma which should be detectable by incoherent scattering techniques.

Experiments in this direction are in progress.

VI. SUMMARY

The injection of relatively strong electron beams with large energy spread into a high density plasma ($10^{13}/cm^3$) gave no indication for an electrostatic instability of the beam. Anomalous energy losses of the beam at the onset of an instability are believed to be the stabilizing mechanism. Disappearance of the excitation light of the beam at a critical electron density was, however, observed. The origin of this effect is not understood at the present time.

REFERENCES

1. D. H. Cooper and M. Raether, CSL Report I-100 (1961).

2. G. Ascoli, CSL Report R-131 (1961).

3. A. K. Berezin, G. P. Berezina, L. I. Bulotin and Ya. B. Fainberg, Journ. Nucl. Energy Part C (Plasma Physics) $\underline{6}$, 173 (1964).

4. I. F. Kharchenko, Journ. Nucl. Energy Part C (Plasma Physics) $\underline{6}$, 201 (1964).

5. C. Etievant, private communication.

6. W. E. Drummond and D. Pines, Nuclear Fusion, Supplement Part $\underline{3}$, 1049 (1962).

7. H. Fröhlich, Nukleonik $\underline{1}$, 183 (1959).

8. H. E. Singhaus, SRI Technical Report 202 (1963).

9. S. Ichimaru, D. Pines and N. Rostoker, Phys. Rev. Letters $\underline{8}$, 231 (1962).

10. W. E. Drummond, Phys. Fluids $\underline{5}$, 1133 (1962).